Biophysical Journal Volume 107 December 2014 2962–2971

Article

Tetracycline Determines the Conformation of Its Aptamer at Physiological Magnesium Concentrations

Andreas J. Reuss,[1] Marc Vogel,[2] Julia E. Weigand,[2] Beatrix Suess,[2,*] and Josef Wachtveitl[1,*]

[1]Institute of Physical and Theoretical Chemistry, Goethe University Frankfurt am Main, Frankfurt, Germany; and [2]Department of Biology, Technical University of Darmstadt, Darmstadt, Germany

ABSTRACT Synthetic riboswitches are versatile tools for the study and manipulation of biological systems. Yet, the underlying mechanisms governing its structural properties and regulation under physiological conditions are poorly studied. We performed spectroscopic and calorimetric experiments to explore the folding kinetics and thermodynamics of the tetracycline-binding aptamer, which can be employed as synthetic riboswitch, in the range of physiological magnesium concentrations. The dissociation constant of the ligand-aptamer complex was found to strongly depend on the magnesium concentration. At physiological magnesium concentrations, tetracycline induces a significant conformational shift from a compact, but heterogeneous intermediate state toward the completely formed set of tertiary interactions defining the regulation-competent structure. Thus, the switching functionality of the tetracycline-binding aptamer appears to include both a conformational rearrangement toward the regulation-competent structure and its thermodynamic stabilization.

INTRODUCTION

Riboswitches are naturally occurring, structured RNAs capable of controlling gene expression in prokaryotic as well as eukaryotic cells at various levels of gene expression (1,2). Usually, they consist of two domains, an aptamer domain capable of recognizing a ligand with high affinity and specificity and an expression platform, which regulates gene expression by its conformational state. Upon binding, the ligand influences the conformational equilibrium of the aptamer domain, which in turn alters the state of the expression platform, thus modulating gene expression rates. Natural riboswitches are solely RNA based and circumvent the need for protein cofactors for gene regulation. Due to this simplicity, they serve as models for the design of synthetic riboswitches. As an example, in vitro selected aptamers can be exploited to control gene expression in response to small molecule ligands (3–5).

In vivo, numerous parameters influence the functionality of riboswitches like the dynamic range of gene expression in relation to the kinetics and dynamics of ligand binding (6). These parameters in turn strongly depend on the ligand-free state of the aptamer domain, as many aptamer domains are required to adopt a binding-competent conformation before ligand recognition and binding (7). Polyvalent cations, particularly Mg^{2+} ions, play a significant role in structure formation by mediating tertiary interactions (8–11). Accordingly, Mg^{2+} considerably affects the ligand-free state and thereby the ligand-binding abilities of many riboswitches that can be as well naturally occurring (7,12–20) as synthetic (21,22).

The tetracycline-binding aptamer (TC aptamer), which is in the focus of our study, was selected in vitro and optimized by a rational design approach (23,24). It has successfully been applied to control gene expression in *Saccharomyces cerevisiae* (24–27). This is remarkable, because only a small number of in vitro selected aptamers are able to control conditional gene expression in living cells (28). Due to its small size compared to naturally occurring riboswitches, its properties have been extensively studied (23,29–33).

Fig. 1 *A* shows the chemical structure of the ligand TC. The secondary structure of the TC aptamer (Fig. 1 *B*) has been analyzed by various genetic, biochemical, and biophysical approaches including structural probing, the tertiary structure was resolved by x-ray crystallography and pulse electron paramagnetic resonance measurements (Fig. 1, *C–E*) (23,29–32). The aptamer consists of three stems (P1, P2, and P3), two loops (L2 and L3), and two single-stranded joining regions (J1/2 and J2/3) as depicted in Fig. 1 *B*.

The TC aptamer binds its ligand with high affinity and specificity at Mg^{2+} concentrations of 3 mM and higher, but the ligand does not bind at all without Mg^{2+}. The high binding affinity is reflected in the dissociation constant K_d of 770 pM ($[Mg^{2+}] = 10$ mM), which is the lowest one reported to date for an in vitro selected RNA aptamer binding to a small molecule (30). The binding pocket is formed by the single-stranded regions J1/2, J2/3, and L3. The hydroxyl group at the $R_{6\beta}$ position of TC (indicated by the *arrow* in Fig. 1 *A*) is important for tight binding as it forms two hydrogen bonds with adenine A13 (one with N3 in the

Submitted August 8, 2014, and accepted for publication November 3, 2014.

*Correspondence: wveitl@theochem.uni-frankfurt.de or bsuess@bio.tu-darmstadt.de

Editor: Michael Sattler.

0006-3495/14/12/2962/10 $2.00

http://dx.doi.org/10.1016/j.bpj.2014.11.001

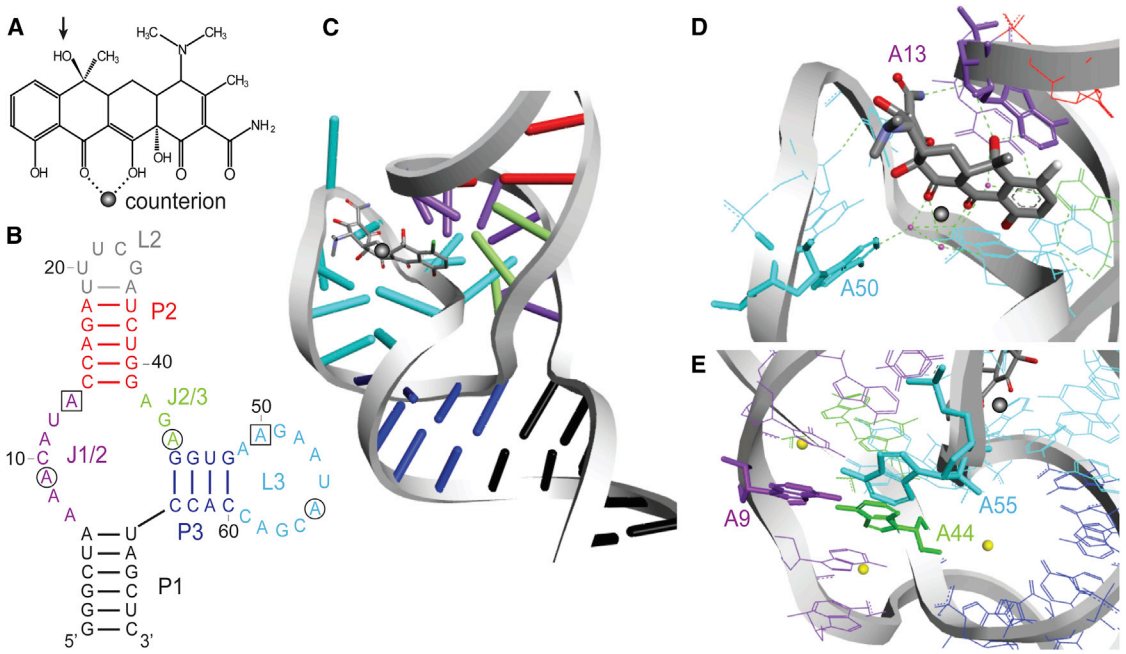

FIGURE 1 (*A*) Chemical formula of TC along with the chelation site for divalent cations. The arrow indicates the hydroxyl group at position $R_{6\beta}$. (*B* and *C*) Illustrate the secondary (*B*) and tertiary (*C*) structures of the TC aptamer. (*D* and *E*) Close-up of the ligand binding pocket. The three stems P1–3, the two junctions J1/2 and J2/3, and the two loops L2 and L3 are color-coded. The loop L2 closing stem P2 is not important for TC binding and omitted in the tertiary structure. (*B*) Nucleotides that are highlighted in (*D*) and (*E*) are indicated with squares and circles, respectively. (*E*) Shows the irregular triple helix, which is a necessary element of the binding-competent structure. The three highly coordinated Mg^{2+} ions in this region are represented as yellow spheres, water molecules have been omitted for clarity. Figs. (*C–E*) are based on the PDB structure 3EGZ (31).

nucleotide and the other one with the 2′-OH group of the ribose; Fig. 1 *D*) (31). TC is bound as a Mg^{2+} chelate forming interactions with residues A49, A50, G51, U54, and A58 mediated by octahedrally coordinated, highly localized water molecules. At least three additional, partially dehydrated and strongly located Mg^{2+} ions could be identified that are heavily involved in stabilizing the irregular triple helix. Several other water molecules further mediate stabilizing tertiary interactions in the binding pocket. Roughly 70% of TCs total accessible surface area is buried within the binding pocket (31).

The structural basis of the complex is formed by an irregular triple helix consisting of the joining regions J1/2 and J2/3 and some nucleotides of loop L3 (31). The three adenines A9, A44, and A55, which are highlighted in Fig. 1 *E*, form a base triplet that stabilizes the triple helix and closes the stem P1. From structural probing and pulse electron paramagnetic resonance experiments ($[Mg^{2+}]$ = 5 mM), it is known that the aptamer is largely preformed in the absence of its ligand. Addition of TC induces local conformational changes in the binding pocket, stabilizing the tighter conformation out of two competing alternatives (23,29,32). Fluorescence-based stopped-flow experiments in 10 mM Mg^{2+} solution showed an extremely fast and unusual two-step binding behavior of TC with a reversible first and an irreversible second step (33). The first step caused an increase of fluorescence emission of ~50% of the total signal change, indicating a strong restriction of the vibrational dynamics of TC already upon initial docking with the RNA. The second step was interpreted as local rearrangement of the binding pocket, necessary to prevent a possible release of the ligand on the time frame of the experiment, which implies that the fully formed complex is stable on a timescale of seconds to minutes.

Previous studies on the TC aptamer show that ligand binding appears not to be accompanied by large conformational changes (32,33). Yet, findings in other synthetic riboswitches suggest that at least some significant reorganization of the RNA appears to be necessary to turn a high affinity aptamer into a functional riboswitch in vivo (34,35). In addition, a prerequisite for usage of an aptamer as riboswitch in vivo is that binding and structural reorganization function in the cellular environment, namely under physiological Mg^{2+} concentrations (36). In an attempt to resolve the apparent contradiction, why the TC aptamer works in vivo, although there seems to be no major structural reorganization involved in ligand binding, we investigated the influence of ligand binding on the structure and stability of the TC aptamer at physiological Mg^{2+} concentrations around 0.5 mM (37–39). Therefore, we performed circular dichroism (CD) spectroscopy, melting studies, and isothermal titration calorimetry (ITC) in both, presence and absence of TC, at varying Mg^{2+} concentrations. We found that the folding transition of the aptamer is driven by Mg^{2+}.

However, folding requires significantly less Mg^{2+} in the presence of TC and completely saturates at Mg^{2+} concentrations between 1 and 2 mM. Additionally, the thermal stability is strongly affected by both, the concentration of Mg^{2+} and the presence of TC.

MATERIALS AND METHODS

Preparation and purification of RNA

For all experiments, RNA was transcribed in vitro using a *Hin*dIII linearized plasmid as template. The plasmid codes for the T7 promoter followed by the aptamer sequence and a self-cleaving hepatitis delta virus (HDV) ribozyme, to ensure homogeneous 3′-ends (the full plasmid sequence is available upon request). In vitro transcription was performed at 37°C overnight in a total volume of 10 ml 20 mM magnesium acetate (0.2 M Tris-HCl pH 8.0, 20 mM DTT, 2 mM spermidine, 0.2 mg/ml linearized plasmid, 4 mM of each NTP, 7.5 μg/ml of T7 polymerase (made in-house)). After transcription, precipitated pyrophosphate was pelleted by centrifugation and 10% (v/v) EDTA (0.5 mM, pH 8.0) was added to the supernatant. After ethanol precipitation, we performed a denaturing polyacrylamide gel electrophoresis (8% PAA, 8 M urea. The RNA was detected via ultraviolet (UV) shadowing, cut out, and eluted from the gel in 0.3 M sodium acetate pH 6.5 at 4°C overnight. To remove the remaining gel slices, the supernatant was filtered using a 0.45 μm filter (Sarstedt, Nümbrecht, Germany) and again the RNA was precipitated using ethanol. Finally, the RNA was resolved in double-distilled water and stored at −20°C.

Sample preparation

All experiments were performed in 20 mM sodium-cacodylate buffer (80 mM NaCl, pH 6.8). This resulted in a total sodium concentration of 100 mM. RNA concentrations were determined by the 260 nm absorption maximum in distilled water using a ND-1000 spectrophotometer (Thermo Fischer Scientific, Wilmington, DE) and then added in appropriate volumes from stock solution to the final buffer solutions. Aqueous TC and doxycycline (DOX) (Sigma-Aldrich, St. Louis, MO) solutions were freshly prepared when needed to prevent hydrolysis. Ligand concentrations were adjusted spectroscopically using the extinction coefficients of TC (355 nm, 13320 l/mol/cm) and of DOX (351 nm, 13180 l/mol/cm).

UV-absorption measurements were performed on a Jasco V-650 spectrophotometer (Jasco Germany, Groß-Umstadt, Germany) in (10 × 4) mm (1 ml) UV-proof fused-silica absorption cuvettes (Hellma Analytics, Müllheim, Germany). Total absorption was (0.5–0.8) oD at 260 nm. Fluorescence emission spectra were recorded on a FLUOROLOG FL3-22 spectrofluorometer (HORIBA Jobin Yvon, Unterhaching, Germany) in (10 × 2) mm UV-compatible fluorescence emission cuvettes (Hellma Analytics) to avoid reabsorption. Source and detector bandwidths were always set to 2.5 nm. The excitation was centered at 375 nm, emission was recorded from 390 to 690 nm. The RNA concentration was 1.5 μM. CD measurements were performed on a Jasco J-710 spectropolarimeter (Jasco Germany) in UV-absorption cuvettes (Hellma Analytics). Optical path lengths of 2, 4, and 10 mm were used for 7.5, 4.5, and 1.5 μM RNA ((0.5–0.8) oD at 260 nm). The ligand concentration was 7.5 μM. Fluorescence-based K_d-measurements were performed and evaluated as described previously (30) at 0.3 and 0.8 mM Mg^{2+}. Minor deviations from the described protocol were slit widths of 4 nm, an integration time of 0.1 s, and a waiting time between individual measurements of 4 min. TC concentrations were 25 and 0.5 nM at 0.3 and 0.8 mM Mg^{2+}, respectively. From the dissociation constants the change of the binding free energy between the two Mg^{2+} concentrations was calculated via $\Delta(\Delta G^o_{i,j}) = -R \cdot T_o \cdot \ln(K_i/K_j)$, where R is the molar gas constant, T_o is 298 K, and K_i and K_j denote the dissociation constants. Its error stems from Gaussian error propagation.

Magnesium titrations

Magnesium titrations were performed by stepwise addition of 2 μl of suitable Mg^{2+} solutions with a Hamilton MICROLITER syringe (Hamilton Bonaduz, Bonaduz, Switzerland) with a maximal volume of 5 μl at 25°C. After addition of the titrant, the cuvette solution was thoroughly mixed and equilibrated for 3 min for each data point. Titrations have been monitored by UV-absorption measurements from 220 to 330 nm and by CD measurements from 220 to 320 nm, respectively. The signal maxima ((260 ± 5) nm for absorption and (270 ± 2) nm for CD) against [Mg^{2+}] were plotted and evaluated. The intersection of the minimal and maximal concentration slopes yield an estimate for the characteristic number of Mg^{2+} ions necessary to induce folding of the aptamer into the native state. Total volume change was <5% and dilution was corrected mathematically. Vertical error bars represent the standard deviation of all replicate titrations performed (at least two in each case), horizontal error bars are calculated from the cumulative uncertainty of the titration syringe using Gaussian error propagation. The influence of titrating Mg^{2+} into TC alone was found to be within experimental error for absorption and CD experiments under the conditions chosen. This is mainly because the total oD of TC was <0.1 with Mg^{2+}-induced changes being much smaller and the K_d of Mg^{2+} binding to pure TC is relatively high (3 mM) (40). Therefore, no separate correction of the TC background was performed.

Melting profiles

UV and fluorescence-monitored melting profiles were recorded for 1.5 μM aptamer with no or 7.5 μM ligand. De- and renaturation profiles were recorded with a temperature gradient of 1°C/min and one data point per °C in the temperature interval from 20°C to 80°C. De- and renaturation curves were averaged to compensate for hysteresis effects. Fluorescence emission of TC was recorded in 0.8 mM Mg^{2+}, UV-absorption experiments at 260 nm were performed for a series of Mg^{2+} concentrations between 0 and 2 mM.

From the melting profiles, apparent folding free energies ΔG^o_a were calculated with a van 't Hoff evaluation scheme (41). This includes fitting upper and lower baselines to the melting curves to calculate the fraction of folded aptamer. For UV-monitored melting, the upper baseline had an inherently high uncertainty, as the presence of Mg^{2+} prevented the recording of melting curves at >80°C. For higher temperatures, too large fractions of the aptamer were hydrolyzed masking the specific melting behavior of the intact aptamer. Therefore, each melting curve was evaluated three times with a best and two extreme upper baselines (a very flat and a very steep one). The slope of the flat baseline was set to zero and one of the steep baselines was set to two times the best value, to ensure that the true baseline is within the considered slope range. Error estimation is based on the variation of the fitted folding free standard enthalpies ΔH^o and entropies ΔS^o derived from all three evaluations. Uncertainties are mainly affected by the quality of the baseline correction and by the extent to which the melting behavior resembles a two-state transition. The relatively large uncertainty at 0.2 and 0.3 mM Mg^{2+} is because in this concentration range, especially with TC, tertiary interactions begin to play a significant role, but are not yet clearly dominant. There, a complicated mixture of occurring states is directly reflected in the error bars. The apparent folding free energies were calculated according to $\Delta G^o_a = \Delta H^o - T_o \cdot \Delta S^o$, where T_o is 298 K and its error stems from Gaussian error propagation with the uncertainties in ΔS^o and ΔH^o.

ITC measurements

ITC experiments were carried out on an iTC200 microcalorimeter (MicroCal, GE Healthcare, Chalfont St. Giles, UK) at 25°C. The sample cell (0.2 ml) contained the RNA and the syringe contained the titrant (Mg^{2+} or TC). After preequilibration and an initial delay of 180 s, a first injection

of 0.2 μl was performed, followed by 15 serial injections (2.5 μl each) with spacing of 180 s. Stirring speed was 1000 rpm and the reference power was 6 μcal/s. Data were recorded as power (μcal/s) over time (min). Afterward, the heat associated with each titration step was integrated and plotted against the molar ratio between the titrant and the RNA. Each binding isotherm was background corrected for dilution effects. Mg^{2+} titrations were fitted to a cooperative Hill-type binding model. As ITC measures the differential heat change *dH* upon titrant addition, the first derivative with respect to [Mg^{2+}] (here:*x*) was used as follows.

$$dH(x) = H_0 \cdot n \cdot k^n \cdot x^{n-1} / (k^n + x^n)^2 \qquad (1)$$

H_0 is the total heat of the saturated titration, *n* is the Hill-coefficient, and *k* is the titrant concentration, where 50% of saturation is reached. At 0.3 and 0.8 mM Mg^{2+}, binding enthalpies were measured with 0.15 and 0.2 mM [TC] as titrant, respectively.

RESULTS

TC aids Mg^{2+}-induced folding

Our aim was to investigate the behavior of the TC aptamer at different Mg^{2+} concentrations. Therefore, we performed different Mg^{2+} titration experiments in the presence and absence of TC. We monitored the transitions by measuring the folding heat directly accessing information about the folding free energies via ITC and changes in the UV-absorption and CD signal reporting on the tertiary structural rearrangements of the aptamer.

In the ITC, titration with Mg^{2+} caused heat bursts indicative of aptamer folding, emerging tertiary interactions and, if present, binding of TC (Fig. 2 *A*). In the presence of TC (*open diamonds*), the binding process starts at lower Mg^{2+} concentrations and the transition saturates faster compared to the titration without ligand (*solid squares*). Fitting Eq. 1 to the ITC experiments yields almost identical Hill-coefficients of 2.54 $\pm$ 0.14 (no TC) and 2.4 $\pm$ 0.2. As the Hill equation is known to rather underestimate the number of binding partners than to overestimate it (42,43) and because the Coulomb-interaction of Mg^{2+}-ions with each other usually results in anticooperative binding behavior (44,45), at least three magnesia are likely to interact with one aptamer in both cases, but it could be significantly more. This finding makes it possible that the same number of Mg^{2+} ions per aptamer molecule is needed to generate the native fold of the aptamer in both cases. The characteristic Mg^{2+} concentrations (*k*-values) are (340 $\pm$ 20) μM and (68 $\pm$ 2) μM, respectively, which means that the ratio of the bulk Mg^{2+} required to induce the folding transition in the absence compared to the presence of TC is 5.0 $\pm$ 0.4. Please note that the bulk concentration of Mg^{2+} behaves completely different as compared to the apparent number of ions needed per aptamer. The folding free enthalpies are ($-$25 $\pm$ 2) kcal/mol (no TC) compared to ($-$46 $\pm$ 4) kcal/mol. The relatively poor quality of the fit to the data with TC at higher Mg^{2+} concentrations is attributed to the onset of a different interaction mode with the aptamer after the actual folding transition into the complexed state is largely finished.

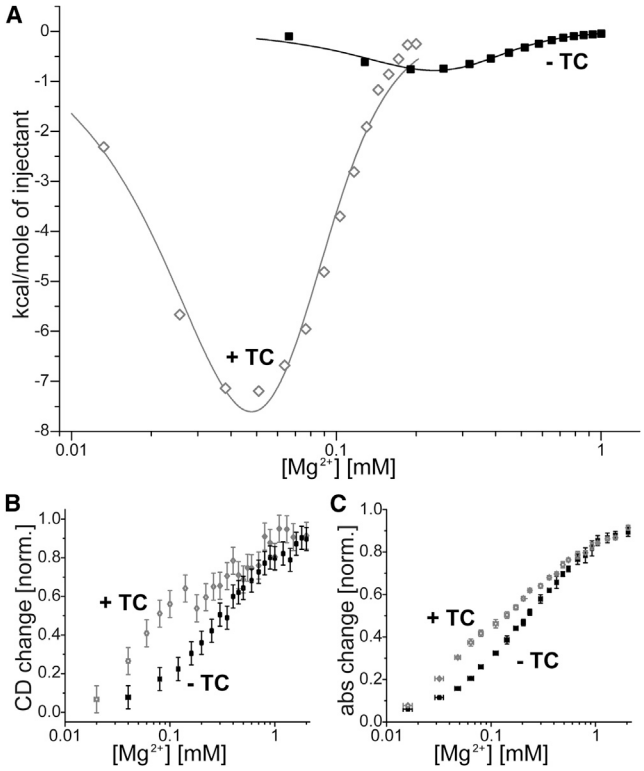

FIGURE 2 (*A*) ITC-monitored heat bursts observed upon stepwise addition of Mg^{2+} in the presence (*gray open diamonds*) and absence (*black solid rectangles*) of TC along with fits (*solid lines*). Data points in (*B*) and (*C*) are coded as in (*A*). (*B*) Normalized changes of the CD signals at 270 nm upon stepwise addition of Mg^{2+} for 1.5 μM aptamer. (*C*) Normalized and inverted change of the absorption signal at 260 nm under conditions identical to (*B*).

CD and UV absorbance spectroscopy are well established and sensitive tools to monitor even subtle changes in tertiary structural rearrangements in RNA (46–48). Titration of 1.5 μM TC aptamer with Mg^{2+} solution causes a rise in the amplitude of the CD signal from 210 to 310 nm, irrespective of the presence or absence of TC. The amplitude is maximal around 270 nm and shifts to longer wavelengths by 4 nm upon addition of Mg^{2+}. The normalized change of the CD signal at 270 nm is shown in Fig. 2 *B*. The signal rises faster in the presence of TC. These experiments have also been performed with 4.5 and 7.5 μM aptamer under otherwise identical conditions (data not shown). These experiments have been evaluated with respect to the number of Mg^{2+} ions needed to drive the folding transition with and without TC and agree with the titration with 1.5 μM aptamer and the absorption-monitored titrations. Fig. 2 *C* shows the identical experiment as in Fig. 2 *B*, but monitored with UV absorption around 260 nm. Absorbance decreased monotonically in the whole spectral range measured upon addition of Mg^{2+} solution. For Fig. 2 *C*, the signal change has been inverted and normalized. Comparing the apparent numbers of Mg^{2+} ions that are necessary to induce the folding transition in the absence and presence of TC yields a ratio of 4 $\pm$ 1

from all spectroscopic experiments mentioned previously. This result agrees well with the ITC experiments.

For all RNA concentrations tested, the total amount of Mg^{2+} ions needed to induce folding was found to be smaller than 0.2 mM. In the presence of TC, only 20% to 25% of the Mg^{2+} amount is needed compared to the situation without the ligand. The titrations indicate two things: i), Mg^{2+}-induced folding of the aptamer is more cooperative in the presence of the ligand and ii), the influence of TC on the tertiary structural rearrangements is particularly large in the range of physiological conditions as complete signal saturation in the absence of tetracycline is reached only at Mg^{2+} concentrations higher than 1 mM.

Tetracycline stabilizes the folded state over a vast temperature range

To learn more about the thermodynamic parameters governing the stability of tertiary structures in the TC aptamer, we performed melting experiments monitored at 260 nm with and without TC at varying Mg^{2+} concentrations from 0 to 2 mM. UV-absorption reports changes in the tertiary RNA structure at different temperatures (41,48). The total change in absorption was ~20% in all cases. The fluorescence emission of TC is known to strongly depend on whether it is bound to the aptamer, or not (30,32,33). This is reflected in a total signal decrease upon dissociation of roughly one order of magnitude, whereas the emission of the pure ligand shows virtually no temperature dependence (Fig. S1 in the Supporting Material).

Fig. 3 *A* shows the melting profiles for $[Mg^{2+}] = 0.8$ mM, Fig. 3 *B* shows the derivatives of these melting curves. Fig. 3, *A* and *B*, have identical coding for the data sets. The rise in absorbance starting above 50°C for the sample with TC (Fig. 3 *A*, *open diamonds*) is reflected in the sharp decrease in fluorescence in the same temperature range (Fig. 3 *A*, *solid line*). An evaluation of the folding free energies according to the van 't Hoff method (41) gives apparent standard folding free energies ΔG_a^o of (-7.4 ± 1.4) kcal/mol for the absorption-detected melting curve and of (-8.4 ± 1.2) kcal/mol for fluorescence-detected melting, respectively. These values agree reasonably well, implying that the steep transition in the absorption-monitored melting curve senses the dissociation of the complex. Additionally, it shows that the UV-absorption curves can be used to estimate the folding free energies in the presence of the ligand quite accurately, although the temperature-induced unfolding obviously is not a simple two-state transition. The values derived with this method rather seem to underestimate ΔG_a^o slightly than overestimating it. The absorbance-detected melting curve without TC deviates strongly from the curve with ligand in the temperature range from 20°C to 60°C. A van 't Hoff analysis of this curve yields an apparent standard free folding energy ΔG_a^o of (-3.0 ± 0.4) kcal/mol, which differs significantly from

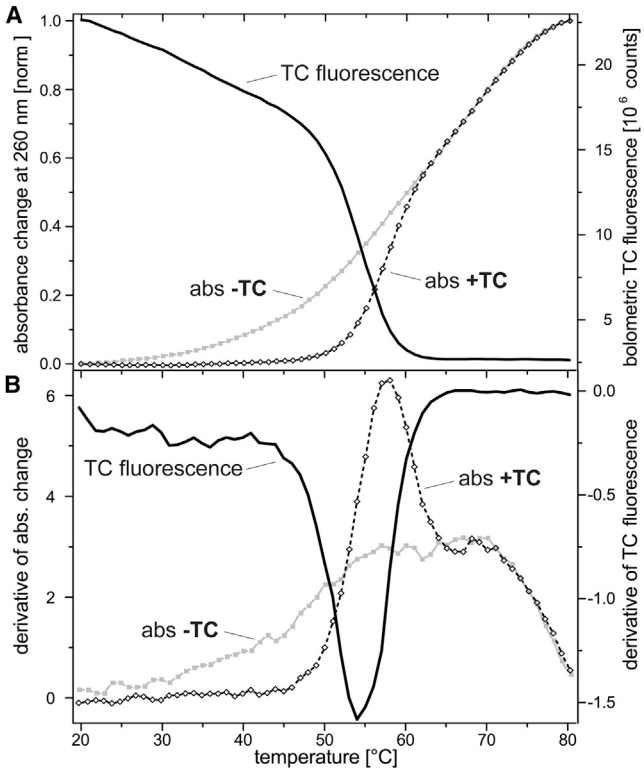

FIGURE 3 (*A*) Melting behavior of the TC aptamer with and without TC at $[Mg^{2+}] = 0.8$ mM is monitored via UV absorption and fluorescence emission spectroscopy. The black line without symbols represents fluorescence emission. Solid gray squares connected with solid lines represent the change in UV absorption at 260 nm in the absence of TC and open black diamonds connected with dashed lines in its presence, respectively. 3 (*B*) Derivatives of the melting curves shown in (*A*). Data sets are coded as in (*A*).

the values found for the aptamer with TC. For temperatures above 60°C (Fig. 3 *A*, *solid squares*), the normalized melting profiles show no differences. This suggests that here the complex and along with it the tertiary structure have already been melted and only unfolding of residual secondary structure and unstacking of nucleotides in single-stranded regions are observed (49–51).

In Fig. 3 *B*, the specific differences in the melting behavior become even more apparent. The aptamer without TC melts over a very broad temperature range and shows little structure, whereas the aptamer with TC shows a well-defined maximum around 57°C and then adopts the melting behavior of the pure aptamer after dissociation of the complex. The maximum in the derivative of the absorbance-monitored melting curve with TC corresponds to a similar minimum in the derivative of the fluorescence-monitored melting with a peak around 54°C. The slight deviation between the peak temperatures may have several reasons. First, fluorescence and absorption monitor two different processes, namely the quenching of TC emission due to the dissociation of the complex as opposed to the change in aptamer absorbance. The exact melting point of the complex is

likely to be masked in the latter case, because the melting behavior of the complex changes into that of the pure aptamer. Second, neither the fluorescence, nor the absorption curves are baseline corrected, which may affect the exact position of the extremum in the derivative (41).

As control, we measured the melting curve of an aptamer mutant (A9G), which cannot adopt the preformed structure (33). Replacing the adenosine at position 9 with a guanosine destroys the base-triplet that forms the structural basis of the preformed aptamer, but keeps the binding pocket intact. Also as control, we melted the wild-type (WT) aptamer with DOX. DOX is a close analog of TC, but lacks the $R_{6\beta}$-OH and shows therefore strongly impaired binding properties (30). All control experiments were performed at 0.8 mM Mg^{2+}. None of these melting profiles show the steep rise in absorbance above 50°C characteristic for melting of the complex (Fig. S2). Their temperature-dependent profiles rather resembles those of the WT aptamer in the absence of TC. The A9G mutant yields ΔG_a^o-values of (-2.3 ± 0.5) kcal/mol and (-3.6 ± 0.5) kcal/mol in the presence and absence of tetracycline, respectively. The WT aptamer in the presence of DOX yields a folding free energy of (-2.4 ± 0.5) kcal/mol. Within their error margins all of these values agree with the one for the WT aptamer without TC. Melting curves with ligand and impaired binding competence generally result in less favorable ΔG_a^o-values than melting without ligand.

TC and Mg^{2+} significantly affect the thermodynamic stability of the TC aptamer

We recorded a series of UV absorption-monitored melting curves with varying Mg^{2+} concentrations with and without TC to further explore the differences in aptamer stability. Fig. 4 *A* shows representative pairs of melting curves for three different Mg^{2+} concentrations. For both series of experiments, the melting temperature rises with the Mg^{2+} concentration. The full set of melting curves (Fig. S3) shows that 0.2 mM Mg^{2+} is the lowest concentration that clearly shows the characteristic melting behavior of the complex. Fig. 4 *B* contains the ΔG_a^o-values for Mg^{2+} concentrations ranging from 0 to 2 mM. From $[Mg^{2+}] = 0.2$ mM on, the apparent folding free energy rapidly increases with TC and saturates at ~1 mM. The interchanged ordering at 0.1 mM Mg^{2+} is not completely understood, but it agrees with the systematically lowered ΔG_a^o-values observed for the control experiments with the A9G mutant and DOX.

The dissociation constant of the TC aptamer is magnesium dependent

We measured the binding affinity of TC to its aptamer at 0.3 and 0.8 mM Mg^{2+} in a fluorescence-based assay. The experiments are shown in Fig. S4. The K_d-values decreased rapidly upon addition of Mg^{2+} in the submillimolar regime

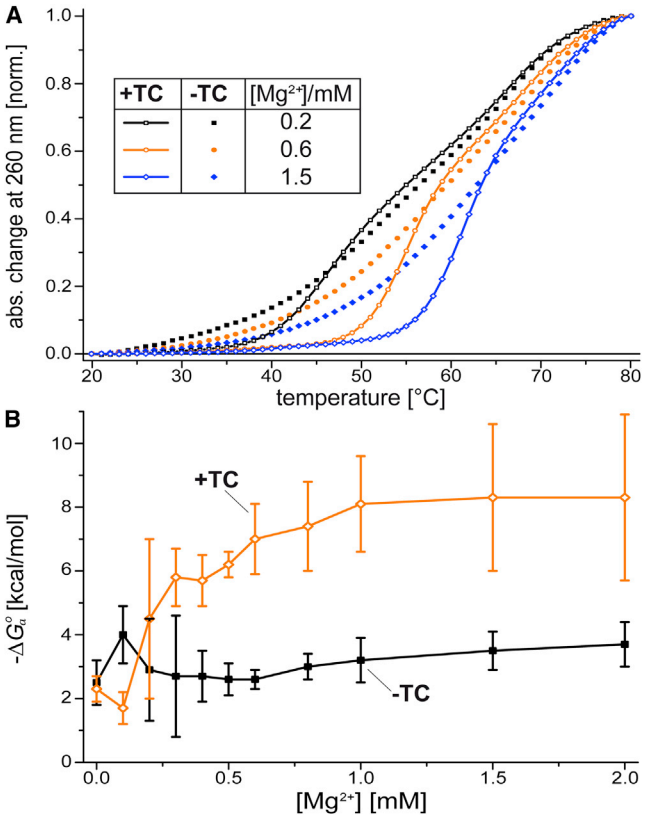

FIGURE 4 (*A*) Representative melting profiles with (*open symbols with solid lines*) and without TC (*filled symbols*) for three different Mg^{2+} concentrations: 0.2 (*black*), 0.6 (*orange*), and 1.5 mM (*blue*). (*B*) The apparent free folding energies ΔG_a^o calculated from the melting profiles with (*orange diamonds*) and without (*black squares*) TC.

from (29 ± 4) nM at 0.3 mM Mg^{2+} to (2.0 ± 0.2) nM at 0.8 mM and continue to decrease further to subnanomolar values for higher Mg^{2+} concentrations as it is known from the literature (30). Accordingly, the standard folding free energy becomes more favorable from 0.3 to 10 mM of Mg^{2+}. From the dissociation constants at 0.3 and 0.8 mM Mg^{2+}, the complex is stabilized by (-1.58 ± 0.11) kcal/mol. This agrees with the change in ΔG_a^o estimated from the melting curves and shown in Fig. 4 *B* from 0.3 to 0.8 mM, which is (-1.6 ± 1.7) kcal/mol. This match is quite noteworthy, considering that the ΔG_a^o-values retrieved from the melting curves essentially report the thermodynamic stability at 55°C and are then extrapolated to 25°C, where base-pairing patterns and stacking interactions are expected to be different compared to room temperature.

Binding experiments in identical buffer conditions were performed with the ITC. The minimal concentration of Mg^{2+} necessary to retrieve a dissociation constant within the sensitivity of the ITC was 0.3 mM (see Fig. S4). The standard binding enthalpies H_0 found in the ITC are (-32 ± 3) and (-19 ± 2) kcal/mol at 0.3 and 0.8 mM Mg^{2+}, respectively. Calculating the corresponding enthalpies from the fit parameters derived in Fig. 2 *A* yields

(−34 ± 5) and (−23 ± 5) kcal/mol, which agree well with the directly measured enthalpies. From the change in the binding energy and the two enthalpies we can learn that the entropic contribution becomes less disfavorable from 0.3 to 0.8 mM Mg^{2+} by (15 ± 4) kcal/mol at 25°C. We attribute this to the fact that folding occurs at 0.3 mM Mg^{2+} from a state with access to the largest parts of the conformational space available to the aptamer: the Mg^{2+} content is large enough to allow for a compact core part of the aptamer and therefore for TC-enforced folding and binding, but it is not sufficient to induce the native tertiary fold on the aptamer on its own. It is likely that complexation is accompanied by a significant loss of conformational freedom, including the conformational freedom of the aptamer itself but also of Mg^{2+} and water molecules necessary to mediate tertiary contacts. At higher Mg^{2+} concentrations it is in turn unlikely for the aptamer to sample very open conformations reducing the effectively available conformational space.

To summarize, we observe no interaction of TC with the aptamer in the absence of Mg^{2+}. In an intermediate range of Mg^{2+} concentrations, TC strongly influences the conformational equilibrium in favor of the regulation-competent state forming the complex. The Mg^{2+}-induced folding occurs at significantly lower salt concentrations in the presence of TC. At the same time, Mg^{2+} and TC both have strong, yet clearly distinguishable impacts on the stability of the aptamer structure, as indicated by melting profiles and K_d-measurements at varying Mg^{2+} concentrations.

DISCUSSION

To unravel the interplay between Mg^{2+} and TC and their interdependent influence on the conformational state of the TC aptamer, a series of spectroscopic and calorimetric experiments was performed under varying solvent conditions. Based on these data, thermodynamic parameters for the interactions of Mg^{2+} and TC with the TC aptamer can be deduced and their significance for the processes that govern the regulatory activity of the TC riboswitch can be analyzed.

TC lowers the Mg^{2+} concentration needed to induce formation of the final tertiary conformation approximately by a factor of four to five. This result has been observed independently with ITC, UV absorption, and CD spectroscopy. It clearly indicates that the role of TC is not purely passive, as indicated by previous results at high Mg^{2+} concentrations. In a regime of moderate Mg^{2+} concentrations (around 0.5 mM), the ligand can induce complex formation accompanied by a significant conformational transition. The dissociation constant of free TC and Mg^{2+} in aqueous solution at pH 6.5 to 7 is around 2 mM (40,52). Under our experimental conditions at 1 mM [Mg^{2+}] only 30% of TC is expected to be chelated. Our data show that already five times less Mg^{2+} is sufficient to form the aptamer-TC complex. The dissociation constant of the chelate complex appears to be smaller in the presence of the aptamer, probably because the energetically favorable aptamer-ligand complex stabilizes the chelate. Taking into account the fact that the concentration of unbound Mg^{2+} in living cells is rather between 0.2 and 1 mM (37–39), we can assume that in cells, the aptamer operates in the medium Mg^{2+} regime.

In general, Mg^{2+} is indispensable to compact RNA structure and can enable specific tertiary interactions (44,53). Additionally, the local Mg^{2+} density close to an oligonucleotide is higher than in the bulk and the gradient is governed by the equilibrium between negative density clustered at the oligonucleotide and the Mg^{2+} concentration gradient (54). A series of investigations on the Mg^{2+} dependence of naturally occurring riboswitches suggest that Mg^{2+} concentrations around 0.5 mM are a very common prerequisite for ligand binding (7,12–15,55). From these experiments, it is also apparent that ligand binding induces an additional conformational change in many natural systems, including the possibility of specific tertiary interactions that can only be induced by the cognate ligand (15). Yet, the response pattern of aptamer domains of natural riboswitches to Mg^{2+} and its cognate ligand can be quite different between the different classes of riboswitches and even within classes. Considering the large variety of conditions in different organisms, these differences might be necessary to allow adaption of regulation schemes and efficiencies to the specific demands of the host system (56). One has to be aware that natural riboswitches are usually comparatively large (>100 nucleotides) with an aptamer domain clearly separated from the expression platform. Therefore, Mg^{2+} might not only be necessary for ligand binding, but in some cases rather establishes allosteric behavior between the functional domains of the riboswitch (7). This is in general less likely for synthetic riboswitches, where the two domains are usually closely coupled due to their small size.

Interestingly, the role of Mg^{2+} on small-molecule-binding aptamers varies from case to case. The binding affinity of the malachite-green-binding aptamer to its cognate ligand gets worse with increasing Mg^{2+} concentrations due to the many possible rotamers of the ligand. High Mg^{2+} concentrations slow down and confine the conformational dynamics of the aptamer, thus making it harder for the aptamer to recognize and bind its ligand (57). The neomycin-binding aptamer also shows an increasing K_d with increasing Mg^{2+} concentrations due to the positive charge of neomycin (J.E.W., unpublished data). The theophylline-binding aptamer rather resembles the behavior of the TC aptamer as do many naturally occurring riboswitches. It requires Mg^{2+} concentrations of at least 1 mM for high affinity ligand binding and recognition. In the absence of Mg^{2+} and other divalent cations like Mn^{2+} and Co^{2+}, the binding constant decreases by four orders of magnitude (21,58).

For the TC aptamer, this suggests that in a high-Mg^{2+} environment, the aptamer is preformed up to the point where

mainly the close-to-binding conformation exists, irrespective of the presence of TC (32,33). In a medium Mg^{2+} regime (some hundred μM Mg^{2+} in bulk solution), TC forces the aptamer into the compact conformation and shifts the conformational equilibrium toward the final tertiary structure. This implies, that the tertiary contacts characteristic for the binding-competent conformation, which form in the absence of TC only at higher bulk Mg^{2+} concentrations, can form at lower concentrations in the presence of TC. Upon formation of the close-to-binding conformation, sites with high negative charge density emerge, particularly in the region of the irregular triple helix composed of the junctions J1/2 and J2/3 along with loop L3 (31). At these sites, Mg^{2+} from the bulk might be recruited in the presence of TC at significantly lower bulk concentrations as compared to the situation without TC. The TC-induced stabilization of the folded state has to outweigh several disfavoring factors like entropy. Our data suggest that TC binding additionally has to outweigh the steeper concentration gradient of the Mg^{2+} ions close to the aptamer toward the bulk. Consequently, there appears to be no need for a very high Mg^{2+} concentration and a strongly preformed aptamer for the riboswitch to function. It is even possible that the riboswitch might not be able to function in a high-Mg^{2+} environment, as it would be always in the final tertiary conformation.

The temperature profiles show a strong stabilization of the native form starting at a minimal concentration of ~0.2 mM Mg^{2+}. This can be seen in the steep transition at the melting temperature of the complex, which suggests that close to the melting temperature there is still almost complete complexation. Below the transition temperatures, the complex is completely temperature insensitive, which also supports the idea that the complex is very stable compared to the pure aptamer. The apparent folding free energies derived from the melting profiles support this interpretation. Thus, the complex is energetically strongly favored compared to the pure aptamer in most Mg^{2+} regimes that were experimentally accessible. From our findings, we can conclude that the aptamer is in the folded, functionally active form with a probability that is roughly two to three orders of magnitude higher in the presence of TC at room temperature and physiological Mg^{2+} concentrations.

In this context, we interpret the observed melting behavior in such a way that secondary and tertiary structure in the absence of TC unfold simultaneously and independently from each other over a very broad temperature range, followed by unstacking of the resulting single-stranded regions at very high temperatures. In the presence of TC, the tertiary structure is stabilized and unfolds at a higher temperature. The stabilized tertiary structure in turn stabilizes the secondary structure, because the binding pocket requires the secondary structure to be intact. Only when the thermal energy overcomes the stability of the complex, the aptamer can access again its whole conformational space and melt as it would without TC. Thus, at low temperatures and a sufficiently high Mg^{2+} content, the bare aptamer and the complex are very likely to have a similar predominant geometry, which is in accordance with previous results from size-exclusion chromatography (30). Yet, their thermodynamic properties are massively different. In this light, the steepness of the melting transition with TC reports directly on the very high change in entropy related to this process, which in turn can be interpreted in such a way that some of the thermal fluctuations of many parts of the aptamer and linked to that of water and salt molecules in the direct proximity of the aptamer are suppressed by TC.

The trends found for the differential Mg^{2+} dependence with respect to the presence of TC are robust and significant. The 100 to 1000 times increased likelihood to find the aptamer correctly folded in the presence of TC at physiological conditions suggest a shortened lifetime of the open conformation and a prolonged one of the bound. This is particularly important because expression processes occur on timescales comparable to riboswitch folding, as recently emphasized by Haller et al. (6). Although in vitro experiments at high Mg^{2+} concentrations suggest little conformational influence of TC on the TC aptamer, our findings make it very likely that TC plays a more important and active role in vivo, where the Mg^{2+} concentration is lower. Additionally, in living cells effects like binding competition with the machinery for translation initiation, crowding effects, and the general heterogeneity of salt conditions and temperature regimes in different cell types and species can influence the conformational equilibrium between the complex and the unfolded state (6,59). Consequently, it is common to optimize the thermodynamic stability of several subunits of synthetic riboswitches, including the expression platform, for regulatory efficiency, when it is applied to a new cell environment or regulation scheme (24,25,60–62).

To conclude, our results obtained with spectroscopic and ITC measurements are in agreement with previous work on structure and binding behavior of the TC aptamer and add new, to our knowledge, aspects to the emerging picture of the interactions and interdependencies between the aptamer, Mg^{2+}, and its cognate ligand TC. Our results are summarized in Fig. 5. In absence of both, TC and Mg^{2+}, the aptamer adopts its secondary, but not a defined tertiary structure. The absence of Mg^{2+} prevents that the triple helix as core of the aptamer can be formed implying that Na^{+} alone is not competent of shielding the electrostatic interactions. We came to this conclusion because TC alone does not induce the formation of tertiary interactions in the absence of Mg^{2+} (23,29).

At Mg^{2+} concentrations higher than ~1.5 mM, near-final tertiary structures are induced and shift the conformational equilibrium toward the fully formed final state irrespective of the presence of TC (23,25,30). Without TC, there is already relatively low residual conformational freedom

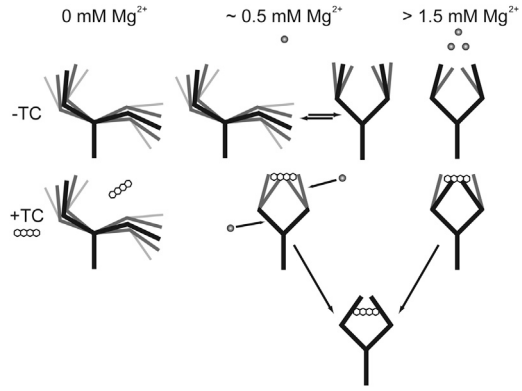

FIGURE 5 The folding behavior of the TC aptamer can be divided into three regimes. At Mg^{2+} concentrations under 70 μM no tertiary interactions and no ligand binding could be observed. At intermediate Mg^{2+} concentrations, the aptamer can sample near-native conformations and bind TC. This process is presumably accompanied by recruitment of Mg^{2+} from bulk to the RNA. At high Mg^{2+} concentrations (>1.5 mM), the aptamer is largely preformed in its binding-competent conformation and tightly binds TC upon rapid complex formation.

left. Still, the binding pocket can adopt at least two competing conformations (32). In this regime, the aptamer can bind TC in a two-step process. Fast initial docking followed by irreversible binding accompanied with local rearrangements of the binding pocket occurs to yield an extraordinarily stable complex (33).

At physiological Mg^{2+} concentrations between 0.2 and 0.8 mM, the interaction pattern somewhat reverts. The aptamer can already form compact structures with tertiary interactions, but Mg^{2+} alone is not yet sufficient to stabilize the native structure as the clearly dominating one (63). The native conformation exists as one out of many potential conformations. The presence of TC in this regime massively biases the conformational equilibrium toward the complex imposing the native tertiary structure on the aptamer. The Mg^{2+} ions necessary to stabilize these tertiary interactions are most likely recruited from bulk solution during the phase of rearrangement. The apparently lowered need for Mg^{2+} to induce aptamer folding in the presence of TC is then the consequence of an increased need for electrostatic screening at negative hot spots created by native tertiary interactions.

SUPPORTING MATERIAL

Four figures are available at http://www.biophysj.org/biophysj/supplemental/S0006-3495(14)01152-7.

The authors thank Dr. C. Grünewald for technical assistance with the absorption and CD spectrometer and Prof. Dr. A. Heckel and Prof. Dr. J. Engels for access to their spectrometers. The authors also thank Dr. M. Hengesbach for fruitful discussion.

This work was supported by the Deutsche Forschungsgemeinschaft CRC902 to B.S. and J.W. and the LOEWE CGT Frankfurt. Funding for the open access charge was provided by the Deutsche Forschungsgemeinschaft.

REFERENCES

1. Breaker, R. R. 2011. Prospects for riboswitch discovery and analysis. *Mol. Cell.* 43:867–879.
2. Serganov, A., and E. Nudler. 2013. A decade of riboswitches. *Cell.* 152:17–24.
3. Wachsmuth, M., S. Findeiß, …, M. Mörl. 2013. De novo design of a synthetic riboswitch that regulates transcription termination. *Nucleic Acids Res.* 41:2541–2551.
4. Rudolph, M. M., M.-P. Vockenhuber, and B. Suess. 2013. Synthetic riboswitches for the conditional control of gene expression in *Streptomyces coelicolor*. *Microbiology.* 159:1416–1422.
5. Ketzer, P., J. K. Kaufmann, …, D. M. Nettelbeck. 2014. Artificial riboswitches for gene expression and replication control of DNA and RNA viruses. *Proc. Natl. Acad. Sci. USA.* 111:E554–E562.
6. Haller, A., M. F. Soulière, and R. Micura. 2011. The dynamic nature of RNA as key to understanding riboswitch mechanisms. *Acc. Chem. Res.* 44:1339–1348.
7. Choudhary, P. K., and R. K. O. Sigel. 2014. Mg(2+)-induced conformational changes in the btuB riboswitch from *E. coli*. *RNA.* 20:36–45.
8. Sosnick, T. R., and T. Pan. 2003. RNA folding: models and perspectives. *Curr. Opin. Struct. Biol.* 13:309–316.
9. Draper, D. E., D. Grilley, and A. M. Soto. 2005. Ions and RNA folding. *Annu. Rev. Biophys. Biomol. Struct.* 34:221–243.
10. Woodson, S. A. 2005. Metal ions and RNA folding: a highly charged topic with a dynamic future. *Curr. Opin. Chem. Biol.* 9:104–109.
11. Soto, A. M., V. Misra, and D. E. Draper. 2007. Tertiary structure of an RNA pseudoknot is stabilized by "diffuse" Mg2+ ions. *Biochemistry.* 46:2973–2983.
12. Yamauchi, T., D. Miyoshi, …, N. Sugimoto. 2005. Roles of Mg2+ in TPP-dependent riboswitch. *FEBS Lett.* 579:2583–2588.
13. Ali, M., J. Lipfert, …, S. Doniach. 2010. The ligand-free state of the TPP riboswitch: a partially folded RNA structure. *J. Mol. Biol.* 396:153–165.
14. Vicens, Q., E. Mondragón, and R. T. Batey. 2011. Molecular sensing by the aptamer domain of the FMN riboswitch: a general model for ligand binding by conformational selection. *Nucleic Acids Res.* 39:8586–8598.
15. Hennelly, S. P., I. V. Novikova, and K. Y. Sanbonmatsu. 2013. The expression platform and the aptamer: cooperativity between Mg2+ and ligand in the SAM-I riboswitch. *Nucleic Acids Res.* 41:1922–1935.
16. Buck, J., J. Noeske, …, H. Schwalbe. 2010. Dissecting the influence of Mg2+ on 3D architecture and ligand-binding of the guanine-sensing riboswitch aptamer domain. *Nucleic Acids Res.* 38:4143–4153.
17. Buck, J., A. Wacker, …, H. Schwalbe. 2011. Influence of ground-state structure and Mg2+ binding on folding kinetics of the guanine-sensing riboswitch aptamer domain. *Nucleic Acids Res.* 39:9768–9778.
18. Haller, A., R. B. Altman, …, R. Micura. 2013. Folding and ligand recognition of the TPP riboswitch aptamer at single-molecule resolution. *Proc. Natl. Acad. Sci. USA.* 110:4188–4193.
19. Suddala, K. C., A. J. Rinaldi, …, N. G. Walter. 2013. Single transcriptional and translational preQ1 riboswitches adopt similar pre-folded ensembles that follow distinct folding pathways into the same ligand-bound structure. *Nucleic Acids Res.* 41:10462–10475.
20. Peselis, A., and A. Serganov. 2014. Themes and variations in riboswitch structure and function. *Biochim. Biophys. Acta. Mech.* 1839:908–918.
21. Zimmermann, G. R., C. L. Wick, …, A. Pardi. 2000. Molecular interactions and metal binding in the theophylline-binding core of an RNA aptamer. *RNA.* 6:659–667.
22. Da Costa, J. B., A. I. Andreiev, and T. Dieckmann. 2013. Thermodynamics and kinetics of adaptive binding in the malachite green RNA aptamer. *Biochemistry.* 52:6575–6583.
23. Berens, C., A. Thain, and R. Schroeder. 2001. A tetracycline-binding RNA aptamer. *Bioorg. Med. Chem.* 9:2549–2556.

24. Suess, B., S. Hanson, …, W. Hillen. 2003. Conditional gene expression by controlling translation with tetracycline-binding aptamers. *Nucleic Acids Res.* 31:1853–1858.
25. Hanson, S., K. Berthelot, …, B. Suess. 2003. Tetracycline-aptamer-mediated translational regulation in yeast. *Mol. Microbiol.* 49:1627–1637.
26. Weigand, J. E., and B. Suess. 2007. Tetracycline aptamer-controlled regulation of pre-mRNA splicing in yeast. *Nucleic Acids Res.* 35:4179–4185.
27. Kötter, P., J. E. Weigand, …, B. Suess. 2009. A fast and efficient translational control system for conditional expression of yeast genes. *Nucleic Acids Res.* 37:e120.
28. Wittmann, A., and B. Suess. 2012. Engineered riboswitches: expanding researchers' toolbox with synthetic RNA regulators. *FEBS Lett.* 586:2076–2083.
29. Hanson, S., G. Bauer, …, B. Suess. 2005. Molecular analysis of a synthetic tetracycline-binding riboswitch. *RNA.* 11:503–511.
30. Müller, M., J. E. Weigand, …, B. Suess. 2006. Thermodynamic characterization of an engineered tetracycline-binding riboswitch. *Nucleic Acids Res.* 34:2607–2617.
31. Xiao, H., T. E. Edwards, and A. R. Ferré-D'Amaré. 2008. Structural basis for specific, high-affinity tetracycline binding by an in vitro evolved aptamer and artificial riboswitch. *Chem. Biol.* 15:1125–1137.
32. Wunnicke, D., D. Strohbach, …, H.-J. Steinhoff. 2011. Ligand-induced conformational capture of a synthetic tetracycline riboswitch revealed by pulse EPR. *RNA.* 17:182–188.
33. Förster, U., J. E. Weigand, …, J. Wachtveitl. 2012. Conformational dynamics of the tetracycline-binding aptamer. *Nucleic Acids Res.* 40:1807–1817.
34. Weigand, J. E., S. R. Schmidtke, …, B. Suess. 2011. Mechanistic insights into an engineered riboswitch: a switching element which confers riboswitch activity. *Nucleic Acids Res.* 39:3363–3372.
35. Duchardt-Ferner, E., J. E. Weigand, …, J. Wöhnert. 2010. Highly modular structure and ligand binding by conformational capture in a minimalistic riboswitch. *Angew. Chem. Int. Ed. Engl.* 49:6216–6219.
36. Carothers, J. M., J. A. Goler, …, J. D. Keasling. 2010. Selecting RNA aptamers for synthetic biology: investigating magnesium dependence and predicting binding affinity. *Nucleic Acids Res.* 38:2736–2747.
37. Raju, B., E. Murphy, …, R. E. London. 1989. A fluorescent indicator for measuring cytosolic free magnesium. *Am. J. Physiol.* 256:C540–C548.
38. Saris, N.-E. L., E. Mervaala, …, A. Lewenstam. 2000. Magnesium. An update on physiological, clinical and analytical aspects. *Clin. Chim. Acta.* 294:1–26.
39. Günther, T. 2006. Concentration, compartmentation and metabolic function of intracellular free Mg2+. *Magnes. Res.* 19:225–236.
40. Martin, S. R. 1979. Equilibrium and kinetic studies on the interaction of tetracyclines with calcium and magnesium. *Biophys. Chem.* 10:319–326.
41. Mergny, J.-L., and L. Lacroix. 2003. Analysis of thermal melting curves. *Oligonucleotides.* 13:515–537.
42. Weiss, J. N. 1997. The Hill equation revisited: uses and misuses. *FASEB J.* 11:835–841.
43. Goutelle, S., M. Maurin, …, P. Maire. 2008. The Hill equation: a review of its capabilities in pharmacological modelling. *Fundam. Clin. Pharmacol.* 22:633–648.
44. Misra, V. K., R. Shiman, and D. E. Draper. 2003. A thermodynamic framework for the magnesium-dependent folding of RNA. *Biopolymers.* 69:118–136.
45. Misra, V. K., and D. E. Draper. 2002. The linkage between magnesium binding and RNA folding. *J. Mol. Biol.* 317:507–521.
46. Pan, T., and T. R. Sosnick. 1997. Intermediates and kinetic traps in the folding of a large ribozyme revealed by circular dichroism and UV absorbance spectroscopies and catalytic activity. *Nat. Struct. Biol.* 4:931–938.
47. Sosnick, T. R., X. Fang, and V. M. Shelton. 2000. Application of circular dichroism to study RNA folding transitions. *Methods Enzymol.* 317:393–409.
48. Pascale, L., S. Azoulay, …, N. Patino. 2013. Thermodynamic studies of a series of homologous HIV-1 TAR RNA ligands reveal that loose binders are stronger Tat competitors than tight ones. *Nucleic Acids Res.* 41:5851–5863.
49. Takach, J. C., P. J. Mikulecky, and A. L. Feig. 2004. Salt-dependent heat capacity changes for RNA duplex formation. *J. Am. Chem. Soc.* 126:6530–6531.
50. Mikulecky, P. J., and A. L. Feig. 2004. Heat capacity changes in RNA folding: application of perturbation theory to hammerhead ribozyme cold denaturation. *Nucleic Acids Res.* 32:3967–3976.
51. Mikulecky, P. J., and A. L. Feig. 2006. Heat capacity changes associated with nucleic acid folding. *Biopolymers.* 82:38–58.
52. Jin, L., X. Amaya-Mazo, …, A. Han. 2007. Ca2+ and Mg2+ bind tetracycline with distinct stoichiometries and linked deprotonation. *Biophys. Chem.* 128:185–196.
53. Pyle, A. M. 2002. Metal ions in the structure and function of RNA. *J. Biol. Inorg. Chem.* 7:679–690.
54. Draper, D. E. 2008. RNA folding: thermodynamic and molecular descriptions of the roles of ions. *Biophys. J.* 95:5489–5495.
55. Montange, R. K., and R. T. Batey. 2008. Riboswitches: emerging themes in RNA structure and function. *Annu. Rev. Biophys.* 37:117–133.
56. Baird, N. J., and A. R. Ferré-D'Amaré. 2010. Idiosyncratically tuned switching behavior of riboswitch aptamer domains revealed by comparative small-angle X-ray scattering analysis. *RNA.* 16:598–609.
57. Sokoloski, J. E., S. E. Dombrowski, and P. C. Bevilacqua. 2012. Thermodynamics of ligand binding to a heterogeneous RNA population in the malachite green aptamer. *Biochemistry.* 51:565–572.
58. Jenison, R. D., S. C. Gill, …, B. Polisky. 1994. High-resolution molecular discrimination by RNA. *Science.* 263:1425–1429.
59. Reining, A., S. Nozinovic, …, H. Schwalbe. 2013. Three-state mechanism couples ligand and temperature sensing in riboswitches. *Nature.* 499:355–359.
60. Suess, B., B. Fink, …, W. Hillen. 2004. A theophylline responsive riboswitch based on helix slipping controls gene expression in vivo. *Nucleic Acids Res.* 32:1610–1614.
61. Kim, D.-S., V. Gusti, …, R. K. Gaur. 2005. An artificial riboswitch for controlling pre-mRNA splicing. *RNA.* 11:1667–1677.
62. Weigand, J. E., M. Sanchez, …, B. Suess. 2008. Screening for engineered neomycin riboswitches that control translation initiation. *RNA.* 14:89–97.
63. Woodson, S. A. 2010. Compact intermediates in RNA folding. *Annu. Rev. Biophys.* 39:61–77.